CORA Cork Open Research Archive
Cartlann Taighde Oscailte Chorcaí

Title	Morphological, compositional, and geometrical transients of V-groove quantum wires formed during metalorganic vapor-phase epitaxy
Authors	Dimastrodonato, Valeria;Pelucchi, Emanuele;Zestanakis, Panagiotis A.;Vvedensky, Dimitri D.
Publication date	2013
Original Citation	Dimastrodonato, V., Pelucchi, E., Zestanakis, P. A. and Vvedensky, D. D. (2013) 'Morphological, compositional, and geometrical transients of V-groove quantum wires formed during metalorganic vapor-phase epitaxy', Applied Physics Letters, 103(4), pp. 042103. doi: 10.1063/1.4816415
Type of publication	Article (peer-reviewed)
Link to publisher's version	http://aip.scitation.org/doi/abs/10.1063/1.4816415 - 10.1063/1.4816415
Rights	© 2013 AIP Publishing LLC..This article may be downloaded for personal use only. Any other use requires prior permission of the author and AIP Publishing. The following article appeared in Dimastrodonato, V., Pelucchi, E., Zestanakis, P. A. and Vvedensky, D. D. (2013) 'Morphological, compositional, and geometrical transients of V-groove quantum wires formed during metalorganic vapor-phase epitaxy', Applied Physics Letters, 103(4), pp. 042103 and may be found at http://aip.scitation.org/doi/abs/10.1063/1.4816415
Download date	2026-11-15 15:50:23
Item downloaded from	https://hdl.handle.net/10468/4282



University College Cork, Ireland
Coláiste na hOllscoile Corcaigh

Morphological, compositional, and geometrical transients of V-groove quantum wires formed during metalorganic vapor-phase epitaxy

Valeria Dimastrodonato, Emanuele Pelucchi, Panagiotis A. Zestanakis, and Dimitri D. Vvedensky

Citation: Appl. Phys. Lett. **103**, 042103 (2013); doi: 10.1063/1.4816415
View online: http://dx.doi.org/10.1063/1.4816415
View Table of Contents: http://aip.scitation.org/toc/apl/103/4
Published by the American Institute of Physics



Morphological, compositional, and geometrical transients of V-groove quantum wires formed during metalorganic vapor-phase epitaxy

Valeria Dimastrodonato,[1] Emanuele Pelucchi,[1] Panagiotis A. Zestanakis,[2] and Dimitri D. Vvedensky[2]
[1]*Tyndall National Institute, University College Cork, "Lee Maltings," Dyke Parade, Cork, Ireland*
[2]*The Blackett Laboratory, Imperial College London, London SW7 2AZ, United Kingdom*

(Received 9 May 2013; accepted 23 June 2013; published online 23 July 2013)

We present a theoretical model of the formation of self-limited (Al)GaAs quantum wires within V-grooves on GaAs(001) substrates during metalorganic vapor-phase epitaxy. We identify the facet-dependent rates of the kinetic processes responsible for the formation of the self-limiting profile, which is accompanied by Ga segregation along the axis perpendicular to the bottom of the original template, and analyze their interplay with the facet geometry in the transient regime. A reduced model is adopted for the evolution of the patterned profile, as determined by the angle between the different crystallographic planes as a function of the growth conditions. Our results provide a comprehensive phenomenological understanding of the self-ordering mechanism on patterned surfaces which can be harnessed for designing the quantum optical properties of low-dimensional systems. © *2013 AIP Publishing LLC*. [http://dx.doi.org/10.1063/1.4816415]

The epitaxial growth of low-dimensional nanostructures on nonplanar substrates has led to the wide-ranging synthesis of integrated optoelectronic and quantum optics building blocks[1–6] by exploiting the variations of the growth rates on the exposed crystallographic planes. The actual material composition can be modulated through growth conditions mediated by kinetics, delivering spatially controllable confinement and, therefore, tuneable electro-optical properties.

V-groove quantum wires (QWRs) grown by metalorganic vapor-phase epitaxy (MOVPE) on patterned GaAs(001) have contributed significantly to the fabrication of ordered and spectrally pure QWR-based lasers and their integration with photonic nanocavities.[7–9] The *in situ* formation of the confined system significantly reduces nonradiative defects at interfaces, leading to increased quantum efficiency when compared with techniques based on etching and regrowth. Despite the broad interest V-groove QWRs have engendered, detailed theoretical modelling at the atomic level of epilayer growth kinetics remains scarce. Analyses of the microscopic surface processes during epitaxial growth can lead to a more complete understanding of facet-dependent thickness and composition, allowing for the more reproducible, on-demand, design of low-dimensional systems.

We have previously presented[10] a phenomenological model with accompanying experimental data for the interplay between precursor decomposition, and the surface diffusion and incorporation of adatoms during the formation of (Al)GaAs V-groove QWRs on patterned GaAs(001) substrates. The appearance of a self-limiting width along the bottom of the groove, together with the segregation of the most mobile adatom species along the vertical axis (perpendicular to the bottom facet) of the recess, produces two-dimensional lateral carrier confinement. Our model, which focusses exclusively on kinetics, in contrast to previous studies,[11,12] provides a complete explanation of the observed behavior in V-groove recesses (e.g., modulation of the self-limiting profile width and Ga segregation) based on (i) different rates of precursor and adatom surface kinetics on each facet plane and (ii) interfacet mass transport, which accounts for growth rate anisotropy and capillarity.

Here, we use our model to analyze the time-dependence of the self-limiting mechanism and Ga segregation during the transient regime. Cross-sectional transmission electron microscopy (TEM)[11] has demonstrated the presence of a transient regime during which the profile of the recess and the Ga segregation evolve toward stationary values determined by the growth conditions and alloy composition. We reproduce the experimentally observed geometric and compositional transients based on reaction-diffusion equations for each facet of the V-groove template, and we explain our results in terms of the surface kinetics established by the geometry and growth conditions. Building on this, we propose a reduced model to explain a poorly understood process in V-groove templates: the evolution of the sidewall angles, which affects lateral confinement and transport properties in QWRs.

Figure 1 shows a schematic illustration of a GaAs(001) substrate patterned with V-grooves and the cross-section of the template used for our theoretical model. The essence of our model is as follows. We simplify the MOVPE process into the following basic steps: the precursors [trimethylgallium/aluminum (group-III) and arsine (group-V)] diffuse through the boundary layer and arrive on the substrate, where, after surface diffusion, they decompose preferentially at step edges,[13] releasing single atoms of the growing material. The atoms then diffuse on the surface until they are incorporated into the growth front. Under our growth conditions, we can neglect kinetics associated with the group-V species,[14] so we include the group-III kinetics only. All precursor and adatom kinetics have different rates on different facets.

The spatio-temporal dependence of the adatom concentration on the ith facet ($i = b, 3, s$ for the (001), (311)A bottom facets and sidewalls, respectively) is given by the reaction-diffusion equation

 © 2013 AIP Publishing LLC

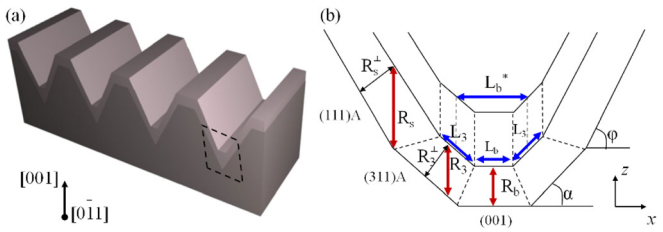


FIG. 1. (a) V-groove array on a GaAs(001) substrate and (b) cross-section of a single V-groove, bounded by (001) bottom, (311)A intermediate, and (111)A sidewall facets. The evolution toward the effective self-limiting profile, $L_b^* = L_b + L_3$, is represented by dashed lines. R_b, R_3, and R_s denote the growth rates on the (001), the (311)A, and (111)A facets, respectively, along the vertical direction z ($R_i^\perp$ are the corresponding components perpendicular to each facet).

$$\frac{\partial n_i}{\partial t} = D_i \nabla^2 n_i + F_i - \frac{n_i}{\tau_i}\,, \tag{1}$$

where D_i is the diffusion constant, F_i the effective atom flux,[10] and τ_i the adatom lifetime to incorporation. D_i and τ_i have Arrhenius forms: $D_i = D_0 \exp(-\beta E_i^D)$, where E_i^D is the barrier for surface diffusion, $\beta = 1/k_B T$, k_B is Boltzmann's constant, and T the absolute temperature, and $\tau_i^{-1} = \nu_i \exp(-\beta E_i^\tau)$,[15] where E_i^τ is the effective barrier for incorporation. All kinetic parameters are listed in Table I. The solution to Eq. (1) enables the growth rates to be calculated as

$$R_i(x) = \frac{dz_i}{dt} = \frac{\Omega_0}{\tau_i} n_i(x)\,, \tag{2}$$

where z_i is the thickness measured along the z axis, Ω_0 is the atomic volume, and x is the spatial coordinate along the facet [Fig. 1(b)]. Continuity of the growth rate at the boundaries between the lateral and bottom facets requires that

$$R_b^{(\mathrm{AlGaAs})}\Big|_{x=\frac{1}{2}L_b} = R_3^{(\mathrm{AlGaAs})}\Big|_{x=\frac{1}{2}L_b} \tag{3}$$

$$= R_s^{(\mathrm{AlGaAs})}\Big|_{x=\frac{1}{2}L_b+L_3}\,, \tag{4}$$

which, in the stationary regime, yields the self-limiting width $L_b^* = L_b + L_3$. Note that the self-limited profile L_b^* can be simplified by assuming that its width is given by the width of the evolving (001) and (311) A facets.[10,17]

TABLE I. Kinetic parameters for Ga and Al adatoms used in Eqs. (5) and (6). These parameters are optimized in relation with those used previously[10] to correct for the new geometry with the basal angles α and φ [see Fig. 1(b)].

Parameter	Al		Ga	
D_0	7.34×10^{-7}	m^2/s	7.34×10^{-7}	m^2/s
ν_i	4.59×10^{-6}	s^{-1}	4.59×10^{-6}	s^{-1}
E_b^D	2.10	eV	1.80	eV
$E_{(311)A}^D$	1.65	eV	1.40	eV
E_s^D	1.60	eV	1.35	eV
E_b^τ	0.040	eV	0.114	eV
$E_{(311)A}^\tau$	0.098	eV	0.128	eV
E_s^τ	0.126	eV	0.159	eV

Equations (3) and (4) determine the evolution of L_b^* during growth, as shown schematically in Fig. 1(b), though their solution requires time-dependent concentrations from Eq. (1). To side-step the direct solution of Eq. (1), we use a method based on the incremental stationary solutions of Eqs. (1) and (2), combined with differential equations for the time-dependence of the width of the (001) (L_b) and (311)A (L_3) bottom facets

$$\frac{dL_b}{dt} = 2\left(R_b - \frac{R_3^\perp}{\cos\alpha}\right)\cot\alpha \tag{5}$$

and

$$\frac{dL_3}{dt} = \frac{\frac{R_3^\perp}{\cos\alpha} - R_b}{\sin\alpha} + \frac{\cos\varphi}{\sin(\varphi-\alpha)}\left(\frac{R_3^\perp}{\cos\alpha} - \frac{R_s^\perp}{\cos\varphi}\right), \tag{6}$$

where all the perpendicular growth rates are functions of L_b and L_3. The dependence of the profile on time is then given by $L_b(t) = L_b(t) + L_3(t)$ [Fig. 1(b)].

Using stationary solutions necessitates choosing an integration time step Δt which allows for the full relaxation of adatom concentrations on each facet.[16] Our choice of kinetic parameters (Table I) implies that (i) the concentrations on the side facet relax in a time given by the adatom lifetime ($L_s \gg \lambda_s$, with $\lambda_s = \sqrt{D_s \tau_s}$ being the surface diffusion length on the sidewalls) and (ii) incorporation and diffusional relaxation on the bottom facet occur over comparable time scales ($L_{b,3} \approx \lambda_{b,3}$, with $\lambda_{b,3} = \sqrt{D_{b,3}\tau_{b,3}}$ being the surface diffusion lengths on the (001) and (311)A facets). For the adatom concentrations to relax on each facet, Δt must be comparable to the longer adatom lifetime. From Table I, we calculate $\tau_{\max} = \tau_s^{\mathrm{Ga}} = 1.45\,\mathrm{s}$ at $T = 973\,\mathrm{K}$, so we choose $\Delta t = 2\,\mathrm{s}$, though shorter time steps $\Delta t \geq 0.9\,\mathrm{s}$ can also be used. This is comparable to the longer adatom lifetime on the (001) facet and highlights the dominance of the kinetics at the bottom of the recess. The stationary solutions of Eq. (1) are used in Eq. (2) to calculate the growth rates which, when cyclically substituted in Eqs. (5) and (6), yield the incremental changes of L_b and L_3. This procedure enables both the geometry and composition of the epitaxial layers to be tracked during growth. The kinetic parameters in Table I (and experimental parameters from Ref. 10) were used for our calculations.

Figures 2(a) and 2(b) show the results for $Al_{0.5}Ga_{0.3}As$ grown on GaAs(001). The widths L_b and L_3 [Fig. 2(a)] show different relaxation times, with L_3 taking longer than L_b to reach the steady state. This behavior is due to the lower incorporation rate of the adatoms on the (311)A than on the (001) facet, resulting in slower surface kinetics and, therefore, a longer transient. Experimental evidence[17] qualitatively confirms this behavior and further validates the phenomenology of our model. The density plot in Fig. 2(b) shows the relative Ga growth rate and Ga segregation along the vertical axis of the template. We clearly observe the Ga enrichment in the middle of the (001) bottom facet. However, the analogous effect, observed on the (311)A facets,[17] does not appear in our model, which instead shows a uniform distribution of Ga-enrichment along the entire width

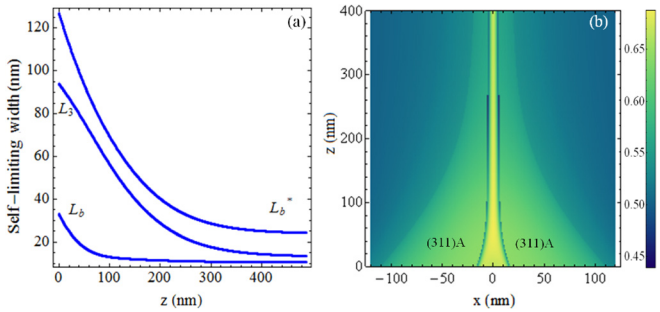


FIG. 2. (a) Widths of the (001) (L_b) and (311)A (L_3) facets and the bottom profile ($L_b^* = L_b + L_3$) as a function of layer thickness (z) for $Al_{0.5}Ga_{0.5}As$ grown on GaAs(001). (b) Density plot of the corresponding relative Ga growth rate. Segregation of Ga appears along the vertical axis of the template (yellow) and the (311)A facets (green). The color bar refers to the calculated relative Ga content. The boundaries are darker because of the discontinuity of the kinetic parameters between adjacent facets.

of the (311)A base. Additional theoretical studies are being carried out to understand this effect.

The change of angle between the facets determining the profile is typical of many epitaxial systems characterized by facet evolution during growth (and/or annealing). Micrographs (atomic force microscopy and TEM) of V-groove structures[17] reveal a clear increase of the angle ϑ between the (001) bottom facet and the (111)A sidewalls with both growth temperature and alloy composition, suggesting a strong relationship between surface kinetics and facet geometry. Previous attempts to explain this behavior postulated a link between the facet step density and the kinetic parameters. We show here that this is not necessary to reach the steady state.

Figure 3(a) illustrates the geometry of our calculation of ϑ. For simplicity, and since we are interested in obtaining the dependence of ϑ on the temperature and composition in the steady state, we employ the stationary solution of the adatom concentrations and growth rates for each facet. The basal angle is defined between the (001) and (111)A facets, so we neglect the intermediate (311)A planes and solve Eqs. (1) and (2) in the stationary regime for only the bottom and lateral facets. Additionally, Eq. (3) will be replaced by

$$R_b^{(\mathrm{AlGaAs})}\Big|_{x=\frac{1}{2}L_b} = R_s^{(\mathrm{AlGaAs})}\Big|_{x=\frac{1}{2}L_b}, \tag{7}$$

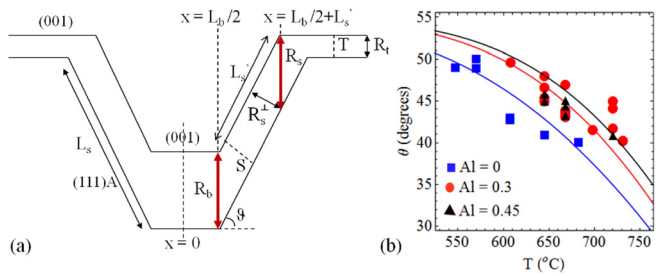


FIG. 3. (a) Schematic representation of the template employed for calculating the angle ϑ between the bottom and lateral facets in the steady state, when the growth rate anisotropy is taken into account (the growth rate R_t on the ridge lower than growth rate R_s on the sidewalls). (b) Experimental data[17] (symbols) and calculated values [Eq. (9)] (solid traces) of ϑ as a function of the growth temperature for the three Al concentrations indicated in the legend.

TABLE II. Kinetic parameters for Ga and Al adatoms used in Eq. (7) for the simplified model without the (311)A facets. We use the same values of D_0 and ν_i as in Table I.

Parameter	Al (eV)	Ga (eV)
E_b^D	2.15	1.90
E_s^D	1.40	1.00
E_b^τ	0.098	0.146
E_s^τ	0.128	0.175

which describes the continuity of the growth rates at the boundaries. The kinetic parameters used for the solution of Eq. (7) are compiled in Table II.

For a complete description of the phenomenology behind the evolution of the profile and the change of ϑ, we must consider the effect of the growth rate anisotropy, which requires that $R_t < R_s^\perp$.[10] We define $R_{ts} \equiv R_t/R_s^\perp$, which allows us to determine the length L_s' of the side facet after growth [Fig. 3(a)], which itself depends on ϑ. Therefore, for each temperature and composition, R_{ts} corresponds to a specific evolution of the length and slope of the sidewalls. The dependence of L_s' on R_{ts} and ϑ is determined by simple geometry [Fig. 3(a)]

$$L_s' = L_s - \frac{\Delta t}{\sin\vartheta}(R_s - R_t), \tag{8}$$

where L_s is the initial (as-etched) length of the sidewalls and $\Delta t R_{s/t}$ the thickness of the layer grown during time Δt on the lateral/top facet (indicated in Fig. 3(a) by S/T). Equation (8) allows us to extract all the growth dynamics related to the bottom, lateral, and top facets. Aside from the explicit dependence of L_s' on the angle and, therefore, on the bottom profile, the dependence of L_s' on R_s and R_t embodies the relation between the surface kinetics on the top and lateral facets and those on the bottom facet. R_s (and $R_t = R_s^\perp R_{ts}$) is indeed a function of L_b [Eq. (7)]. Therefore, despite our simplified treatment, we are able to reproduce the complete phenomenological scenario during deposition. The solution for ϑ is obtained by requiring that the growth rates of the sidewall at the boundary with the bottom ($\frac{1}{2}L_b$) and with the top facets ($\frac{1}{2}L_b + L_s'$) are the same

$$R_s^{(\mathrm{AlGaAs})}\Big|_{x=\frac{1}{2}L_b} = R_s^{(\mathrm{AlGaAs})}\Big|_{x=\frac{1}{2}L_b+L_s'}, \tag{9}$$

where L_s' introduces the unknown ϑ [Eq. (8)] and, through R_{ts}, stipulates that the evolution of the lateral facet is determined by growth rate anisotropy. Previous work[10] revealed that R_{ts} follows the Arrhenius form $R_{ts} = C_{ts}\exp(-\beta E_{ts})$, with $E_{ts} = E_{001} - E_{(111)A}$ being the difference between the decomposition barrier on the top (001) facet and the (111)A sidewalls. The optimized values of C_{ts} and E_{ts} used here are compiled in Table III.

We now consider the time step Δt. Figure 1 suggests a transient time for $Al_{0.5}Ga_{0.5}As$ of ≈1500 s (≈400 nm), while, for higher Ga content, longer transient regimes of ≈6000 s (≈1500 nm) are expected (due to the slower incorporation rate). Starting at $\Delta t = 3000$ s, we have optimized the time

TABLE III. Optimized values of the exponential prefactor C_{ts} and the energy barrier E_{ts} in the Arrhenius form of R_{ts} used in Eq. (9). The growth duration Δt necessary to reach equilibrium on the ridge and sidewall is also shown.

Parameter	Al = 0	Al = 0.3	Al = 0.45
C_{ts}	334.1	1835	2900
E_{ts}	0.60 eV	0.78 eV	0.82 eV
Δt	4500 s	4500 s	4500 s

step based on the best fit to the experimental temperature-dependence of ϑ.

The calculated results are shown in Fig. 3(b) for different Al contents and compared with experimental data. Despite the spread values of the experimental data, the increasing trend of ϑ with temperature can be clearly observed. Our results qualitatively confirm this behavior and reproduce the increase of the steepness of the sidewalls for higher Al contents. For a given alloy composition (T), as T (Ga content) increases, the surface-diffusion-induced capillarity effect causes a higher growth rate along the bottom of the template, leading to a widening of the profile and a flattening of the sidewalls with respect to the initial profile.

In conclusion, we have discussed the time-dependent behavior of the self-limiting mechanism and Ga segregation along the bottom of a V-groove template during MOVPE and reproduced the experimentally observed evolution of the cross-sectional profile, determined by the angle between the (001) bottom and (111)A lateral facets, as functions of the growth temperature and composition. The competition between the facet-dependent kinetic processes, e.g., precursor decomposition, adatom migration, and incorporation, has been analyzed in relation to the geometry of the bounding facets during both the transient and stationary regimes. This scenario represents the foundation for predicting the morphological evolution of the template for a set of growth conditions, allowing for the more reproducible design of nanostructures with specific quantum optical properties.

This research was enabled by the Irish Higher Education Authority Program for Research in Third Level Institutions (2007 to 2011) via the INSPIRE programme, and by Science Foundation Ireland under grant 10/IN.1/I3000.

[1]A. Madhukar, K. C. Rajkumar, and P. Chen, Appl. Phys. Lett. **62**, 1547 (1993).
[2]S. Koshiba, H. Noge, H. Akiyama, T. Inoshita, Y. Nakamura, A. Shimizu, Y. Nagamune, M. Tsuchiya, H. Kano, H. Sakaki, and K. Wada, Appl. Phys. Lett. **64**, 363 (1994).
[3]R. Notzel, Z. Niu, M. Ramsteiner, H.-P. Schonherr, A. Tranpert, L. Daweritz, and K. H. Ploog, Nature **392**, 56 (1998).
[4]E. Kapon, E. Pelucchi, S. Watanabe, A. Malko, M. H. Baier, K. Leifer, B. Dwir, F. Michelini, and M.-A. Dupertuis, Physica E **25**, 288 (2004).
[5]E. Pelucchi, V. Dimastrodonato, L. O. Mereni, G. Juska, and A. Gocalinska, Curr. Opin. Solid State Mater. Sci. **16**, 45 (2012).
[6]G. Juska, V. Dimastrodonato, L. O. Mereni, A. Gocalinska, and E. Pelucchi, Nat. Photonics **7**, 527–531 (2013).
[7]E. Kapon, J. P. Harbison, C. P. Yun, and N. G. Stoffel, Appl. Phys. Lett. **52**, 607 (1988).
[8]E. Kapon, D. M. Hwang, and R. Bhat, Phys. Rev. Lett. **63**, 430 (1989).
[9]K. A. Atlasov, A. Rudra, B. Dwir, and E. Kapon, Opt. Express **19**, 2619 (2011).
[10]E. Pelucchi, V. Dimastrodonato, A. Rudra, K. Leifer, E. Kapon, L. Bethke, P. A. Zestanakis, and D. D. Vvedensky, Phys. Rev. B **83**, 205409 (2011).
[11]G. Biasiol and E. Kapon, Phys. Rev. Lett. **81**, 2962 (1998).
[12]M. Ozdemir and A. Zangwill, J. Vac. Sci. Technol. A **10**, 684 (1992).
[13]T. Shitara, T. Kaneko, and D. D. Vvedensky, Appl. Phys. Lett. **63**, 3321 (1993).
[14]P. Chen, J. Y. Kim, A. Madhukar, and N. M. Cho, J. Vac. Sci. Technol. B **4**, 890 (1986).
[15]V. Dimastrodonato, E. Pelucchi, and D. D. Vvedensky, Phys. Rev. Lett. **108**, 256102 (2012).
[16]V. Dimastrodonato, E. Pelucchi, P. Zestanakis, and D. D. Vvedensky, Phys. Rev. B **87**, 205422 (2013).
[17]G. Biasiol, "Formation mechanisms of low-dimensional semiconductor nanostructures grown by OMCVD on nonplanar substrates," Ph.D. thesis (Swiss Federal Institute of Technology, Lausanne, 1998).